Semiclassical Quantization Using Invariant Tori: A Gradient-Descent Approach†

Emmanuel Tannenbaum

Department of Chemistry and Chemical Biology, Harvard University, Cambridge, Massachusetts 02138

Eric J. Heller*

Departments of Chemistry and Physics, Harvard University, Cambridge, Massachusetts 02138

Received: December 4, 2000; In Final Form: January 19, 2001

This paper presents a PDE-based, gradient-descent approach (GDA) to the EBK quantization of nearly separable Hamiltonians in the quasi-integrable regime. The method does this by finding an optimal semiclassical basis of invariant tori which minimizes the angular dependence of the Hamiltonian. This representation of the Hamiltonian is termed an intrinsic resonance representation (IRR), and it gives the smallest possible basis obtainable from classical mechanics. Because our method is PDE-based, we believe it to be significantly faster than previous IRR algorithms, making it possible to EBK quantize systems of higher degrees of freedom than previously studied. In this paper we demonstrate our method by reproducing results from a two-degree-of-freedom system used to demonstrate the previous Carioli, Heller, and Moller (CHM) implementation of the IRR approach. We then go on to show that our method can be applied to higher dimensional Hamiltonians than previously studied by using it to EBK quantize a four- and a six-degree-of-freedom system.

1. Introduction

The semiclassical quantization of D-dimensional nonseparable Hamiltonians is an old and difficult problem. Before the discovery of the Schrodinger equation, the standard procedure was essentially what is known today as the Einstein−Brillouin−Keller (EBK) quantization method. In this method, one looks for canonical momenta $I_1, ..., I_D$, which are invariants of the Hamiltonian, known as the action variables, and then sets these invariants equal to $2\pi\hbar(n_i + \alpha_i/4)$, where the α_i are the Maslov indices. (A system for which such invariants can be found everywhere in phase space is said to be integrable.) The Hamiltonian H depends exclusively on the D actions $I_1, ..., I_D$, and so the semiclassical energies of the Hamiltonian are characterized by good quantum numbers via $E(n_1, ..., n_D) = H(I_1, ..., I_D)$, with $I_i = 2\pi\hbar(n_i + \alpha_i/4)$. Usually $\alpha_i = 2$.

In one-dimension, this procedure is straightforward. There is only one action variable I, and it is given by

$$I = \oint p\,dq \tag{1}$$

where the contour integral denotes integration over one period of the motion, and $p = \pm\sqrt{2m(E-V(q))}$ is the momentum of the particle. It is usually not possible to obtain $I = I(E)$ analytically, and in the case of multiple wells there is more than one I for a given E. Nevertheless, the implementation of this method is relatively straightforward.

This simple scheme fails in higher dimensions. The problem is that for a general nonseparable Hamiltonian, the classical motion may very well be chaotic. No invariants other than the energy can be found, and so the energies cannot be characterized by good actions. On the other hand, if the Hamiltonian is separable, then the problem can be broken down into a series of one-dimensional problems. Because for each degree of freedom the phase space motion traces out a closed curve topologically equivalent to a circle, the overall motion of the whole system lies on what is called an invariant torus. The invariant tori fill out the entire phase space (or at least the region within any kind of dissociation energy of the system). The tori are each characterized by an action vector $I = (I_1, ..., I_D)$, and our system is quantized in the manner described above.

If an integrable system is perturbed, and the perturbation is sufficiently weak, then most of the phase space is still covered by invariant tori.[8] This is essentially the content of the KAM theorem. Thus, it is still possible to find the semiclassical energies using the EBK approach. The complication that arises is the presence of resonances or near-resonances which lead to the formation of resonance zones. Invariant tori still exist inside the resonance zones; however, they are described by a set of action-angle variables that cannot be analytically continued outside the zones. Thus there is no longer any kind of global action-angle description of the Hamiltonian (the angles being the canonical coordinates). The integrable regions of phase space are therefore covered by a collection of action-angle variables, each of which is only locally valid within a certain region of phase space. Still, each of the sets of local actions may be quantized, and by doing so it is possible to construct the full EBK spectrum. The problem with this approach is that quantum mechanically, tori in the different regions of phase space, i.e., separated by resonance zones, are still coupled to each other. (As evidence for this, the Hamiltonian can be evaluated in the EBK states, and the off-diagonal elements are nonvanishing.) The energy flow between such tori is known as dynamical tunneling, and it leads to the breaking of degeneracies or near-degeneracies in the EBK energies. The above method of quantizing the local sets of actions fails to take this into account.

An alternative approach is to remain in a global action-angle basis and to transform to a set of action-angle variables which minimizes the angle dependence of the Hamiltonian. Such a

† Part of the special issue "William H. Miller Festschrift".

10.1021/jp004371d CCC: $20.00
Published on Web 03/02/2001

representation is termed an intrinsic resonance representation (IRR), a term coined by Carioli et al.[1] The angular dependence of a Hamiltonian is minimized when the angular terms are all resonant terms of the zeroth-order Hamiltonian. It is impossible to reduce the angular dependence further, because the resonant terms lead to the formation of resonance zones, which prevent a global action-angle description of the Hamiltonian.

We then use the IRR tori as a semiclassical basis with which to represent our Hamiltonian in matrix form. Because much of the classical dynamics has already been absorbed into the IRR tori, leaving only the quantum transport across resonance zones, it is possible to obtain the semiclassical energies using a much smaller basis than required with a zeroth-order action-angle representation. Furthermore, physical insight is obtained, because the resulting basis is derived from the underlying dynamics of the system, whereas the original basis (e.g., harmonic oscillators) is often chosen for computational convenience.

Carioli, Heller, and Moller (CHM) published an algorithm in 1997 to construct the IRR basis from a given Hamiltonian.[1] Their method was a generalization of the Chapman, Garrett, and Miller (CGM)[2] method for finding invariant tori of a nearly separable system. One drawback with the CHM method is that it requires a priori knowledge of which terms in the Hamiltonian are to be considered resonances, and which terms are not. The CHM method transforms away the nonresonant terms using an iterative scheme that updates the full Hamiltonian at every iteration step. Convergence requires only a few iterations, and the final Hamiltonian contains only the resonant terms. However, often the terms are not exactly resonant, but nearly resonant. In principle, near-resonances are to be treated like resonances. Unfortunately, this is a perturbation-dependent term, and thus there is a certain ambiguity in the transition from regarding a term as nonresonant to resonant.

Another drawback with the CHM method is that at each step, it is necessary to evaluate a multidimensional integral and to invert a nonlinear angle map. These features slow the algorithm down, making it difficult to study systems with more than two or three degrees of freedom.

In this paper we present an alternative approach to finding the IRR basis. This method is essentially a gradient-descent approach (GDA) and does not require any a priori assignment of potential terms as resonant or nonresonant. At each iteration step every term in the Hamiltonian is adjusted depending on how close it is to being resonant. Convergence typically requires 2 to 3 iteration steps (at least on the systems studied in this paper). The method, as implemented in this paper, is nearly as accurate as the CHM algorithm in obtaining the semiclassical energies. Its main advantage is that it avoids evaluating multidimensional integrals or inverting nonlinear angle maps. Thus, we believe that it is much faster than the CHM method, making it possible to find IRR tori in higher degrees of freedom than previously studied.

The paper is organized as follows: In section 2, we give a brief review of the CGM method for finding the invariant tori of a nonresonant system. In section 3, we describe the CHM generalization of the CGM method, which allows one to find the IRR tori of a Hamiltonian. In section 4, we present the gradient-descent method and show that it reduces to first-order perturbation theory in the weakly perturbed limit. In section 5, we describe the numerical implementation of our method. Finally, in section 6 we present our numerical results. We first begin by demonstrating our method using the same two-dimensional Hamiltonian which Carioli et al. used to demonstrate the CHM method.[1] We then go on to show that our method can be used to study higher dimensional systems than previously studied, by looking at four and six dimensional examples.

2. The CGM Method

The CGM method is an iterative algorithm that finds the invariant tori of some Hamiltonian $H(\mathbf{J},\theta)$. It does this by finding a generating function $S(\mathbf{I},\theta)$, transforming from the action-angles $(\mathbf{J},\theta)$ to $(\mathbf{I},\phi)$, so that $H(\mathbf{J},\theta) = \tilde{H}(\mathbf{I})$, where $\tilde{H}$ denotes the representation of H in the new action-angle coordinates.

We start with some integrable D-dimensional Hamiltonian $H_0(\mathbf{J})$, to which we add a small perturbation $V(\mathbf{J},\theta)$, where we can expand V in a Fourier series via

$$V(\mathbf{J},\theta) = \sum_{\mathbf{k}\neq 0} V_k(\mathbf{J}) e^{2\pi i \mathbf{k}\cdot\theta} \tag{2}$$

where $\mathbf{k} = (k_1,...,k_D)$, is a vector of integers.[9] We do not include the zero vector, since this can be absorbed into H_0. Because our perturbation is small, we write $S(\mathbf{I},\theta)$ as $S(\mathbf{I},\theta) = \mathbf{I}\cdot\theta + G(\mathbf{I},\theta)$, where $G(\mathbf{I},\theta) = \sum_{\mathbf{k}\neq 0} G_k(\mathbf{I}) e^{2\pi i \mathbf{k}\cdot\theta}$. The new and old action-angle variables are related to each other via

$$\mathbf{J} = \mathbf{I} + \nabla_\theta G(\mathbf{I},\theta) \tag{3}$$

$$\phi = \theta + \nabla_{\mathbf{I}} G(\mathbf{I},\theta) \tag{4}$$

Therefore, $H(\mathbf{J},\theta) = H(\mathbf{I} + \nabla_\theta G(\mathbf{I},\theta),\theta) = \tilde{H}(\mathbf{I},\theta)$. We can expand $\tilde{H}$ in a Fourier series in θ, writing

$$\tilde{H}(\mathbf{I},\theta) = \sum_{\mathbf{n}} \tilde{H}_k(\mathbf{I}) e^{2\pi i \mathbf{n}\cdot\theta} \tag{5}$$

where

$$\tilde{H}_n \equiv \tilde{H}_n[\{G_k\}](\mathbf{I}) = \int H(\mathbf{I} + \nabla_\theta G(\mathbf{I},\theta),\theta)^{-2\pi i \mathbf{n}\cdot\theta} d\theta \tag{6}$$

where each θ_i is integrated from 0 to 1. The goal of the CGM method is to then choose our $G_k(\mathbf{I})$ so that

$$\tilde{H}_n[\{G_k\}](\mathbf{I}) = 0 \qquad \mathbf{n} \neq \mathbf{0} \tag{7}$$

This is done using a Newton−Raphson iteration scheme, at the end of which we have $H(\mathbf{J},\theta) = \tilde{H}_0(\mathbf{I})$, assuming we obtain convergence.

The beauty of this method is that the actions $\mathbf{I}$ of the final torus are fixed at the start of the algorithm by the user. By setting $\mathbf{I} = 2\pi\hbar(\mathbf{n} + 1/2)$, we readily obtain the EBK spectrum of the Hamiltonian.

3. The CHM Method

The CGM method fails when there are resonances in the Hamiltonian. Because of the formation of resonance zones in the phase space, the CGM representation of the Hamiltonian is a local one, and thus cannot handle quantum effects such as dynamical tunneling. The CHM method, on the other hand, remains in a global action-angle basis even in the presence of resonances. It does this by reducing the angular dependence of the Hamiltonian as much as possible, but not completely, leaving only those angular terms corresponding to resonances and active fast terms.

We illustrate the method in the simplest case, that of a single resonance $\mathbf{r}$. (If $\nu(\mathbf{J})$ denotes the zeroth-order frequencies of the Hamiltonian, then a resonance $\mathbf{r}$ at zeroth-order action $\mathbf{J}$ means that $\nu(\mathbf{J})\cdot\mathbf{r} = 0$. A two-dimensional example is if ν_1-

$(J_1,J_2) = 2\nu_2(J_1,J_2)$, then $\mathbf{r} = (1,-2)$ is a resonance at (J_1,J_2).) The trick is to break the Hamiltonian into two pieces. The first piece consists of all the nonresonant terms, and may be expressed as

$$H_{nr}(\mathbf{J},\theta) = \sum_{\mathbf{n}\neq p\mathbf{r},p\neq 0} H_n(\mathbf{J})e^{2\pi i\mathbf{n}\cdot\theta} \tag{8}$$

The second piece consists of the resonant terms and may be expressed as

$$H_r(\mathbf{J},\theta) = \sum_{p\neq 0} H_{pr}(\mathbf{J})e^{2\pi ip\mathbf{r}\cdot\theta} \tag{9}$$

In the CHM method, we apply a modified CGM method to H_{nr} as follows: The Fourier components of H in the new action-angle variables are given by

$$\tilde{H}_n(\mathbf{I}) \equiv \tilde{H}_n[\{G_k\}](\mathbf{I}) = \int H(\mathbf{I} + \nabla_\theta G(\mathbf{I},\theta),\theta(\mathbf{I},\phi))e^{-2\pi i\mathbf{n}\cdot\phi}d\phi \tag{10}$$

We use the Newton−Raphson method to solve $\tilde{H}_n[\{G_k\}](\mathbf{I}) = 0$, $\mathbf{n} \neq p\mathbf{r}$, $p \neq 0$. At each step of the iteration, the map $\phi^{(n)} = \theta + \nabla_{\mathbf{I}}G^{(n)}(\mathbf{I},\theta)$ is inverted using a procedure developed by Warnock and Ruth.[3] The program is stopped when the nonresonant Fourier components are smaller than some specified error. The resultant Hamiltonian may then be written as

$$\tilde{H}(\mathbf{I},\phi) = \sum_p \tilde{H}_{pr}\, e^{2\pi ip\mathbf{r}\cdot\phi} \tag{11}$$

We then use the resulting tori as a semiclassical basis with which to construct our matrix representation of the Hamiltonian. If we let $|\mathbf{n}\rangle$ denote a basis state corresponding to the torus with actions $\mathbf{I}_n = 2\pi\hbar(\mathbf{n} + 1/2)$, then the semiclassical coupling $\langle\mathbf{m}|\hat{H}|\mathbf{n}\rangle$ is given by

$$\hat{H}_{mn} = H_{\mathbf{m}-\mathbf{n}}\left(\frac{\mathbf{I}_\mathbf{m} + \mathbf{I}_\mathbf{n}}{2}\right) \tag{12}$$

where $H_{\mathbf{m}-\mathbf{n}}$ denotes the $\mathbf{m}-\mathbf{n}$ Fourier component of H.[6] This expression neglects contributions from the classically forbidden region; however, if we are working in a regime in which a semiclassical analysis gives accurate results, then we expect such contributions to be small (because the EBK wave functions decay rapidly outside the classically allowed region).

In the more general case of multiple resonances, these terms must be included into H_r in order to achieve convergence. It may also be necessary to include near-resonances or even fast terms (in the case of chaotic dynamics).

4. The Gradient-Descent Approach

4.1. Problems with the CHM Method. There are two main drawbacks to the CHM method: First, the trick of removing resonant terms from the Hamiltonian runs into trouble in the case of near-resonances. For a stronger perturbation, near-resonances and sometimes even fast terms need to be removed in order for the Newton−Raphson method to converge. However, these excluded terms should still be reduced as much as possible, though not necessarily completely. Because the CHM method fails to do this, it is not clear that it will always give the optimal Hamiltonian with a minimized angular dependence. Only in cases where there are few exact or near-resonances, with the other terms highly nonresonant, will the minimized angular dependence be obtained.

The second disadvantage to the CHM method is that at each iteration step it is necessary to invert the angle map and then to evaluate a multidimensional integral in order to obtain the updated Fourier components of the Hamiltonian. This feature slows the CHM method down, making it difficult to apply to systems with more than two or three degrees of freedom.

The way around all these drawbacks is to continuously deform the original action-angle system via a series of infinitesimal generating functions. Each Fourier component of the Hamiltonian is continuously evolved from some initial value to some final value. The more nonresonant a term, the closer it is brought to zero (where a "resonance" can also mean a fast term that has become active due to the size of the perturbation). Furthermore, by avoiding the need to invert nonlinear functions and to evaluate multidimensional integrals, we can get to the IRR basis much faster than with the CHM method, making it possible to study systems having higher degrees of freedom (up to $D = 6$ in this paper, and possibly higher).

4.2. The Evolution Equation. To derive the PDE governing the evolution of the Fourier components of H, we assume that at some time t in our evolution we have arrived at some action-angle system $(\mathbf{I}_t,\phi_t)$. To propagate to time $t + dt$, we use a generating function $\mathbf{I}_{t+dt}\cdot\phi_t + dtG(\mathbf{I}_{t+dt},\phi_t)$. For ease of notation we shall set $\mathbf{J} = \mathbf{I}_t$, $\mathbf{I} = \mathbf{I}_{t+dt}$, $\theta = \phi_t$, $\phi = \phi_{t+dt}$. Since dt is infinitesimally small, we need only worry about first-order terms. Thus,

$$\mathbf{J} = \mathbf{I} + dt\nabla_\phi G(\mathbf{I},\phi) \tag{13}$$

$$\theta = \phi - dt\nabla_{\mathbf{I}}G(\mathbf{I},\phi) \tag{14}$$

Therefore,

$$\begin{aligned} H^{(t+dt)}(\mathbf{I},\phi) &= H^{(t)}(\mathbf{J},\theta) \\ &= H^{(t)}(\mathbf{I} + dt\nabla_\phi G(\mathbf{I},\phi),\, \phi - dt\nabla_{\mathbf{I}}G(\mathbf{I},\phi)) \\ &= H^{(t)}(\mathbf{I},\phi) + dt(\nabla_{\mathbf{I}}H^{(t)}\cdot\nabla_\phi G(\mathbf{I},\phi) - \\ &\qquad \nabla_\phi H^{(t)}\cdot\Delta_{\mathbf{I}}G(\mathbf{I},\phi)) \end{aligned} \tag{15}$$

and so, we obtain,

$$\begin{aligned} \frac{\partial H(\mathbf{I},\phi)}{\partial t} &= \nabla_{\mathbf{I}}H(\mathbf{I},\phi)\cdot\nabla_\phi G(\mathbf{I},\phi) - \nabla_\phi H(\mathbf{I},\phi)\cdot\nabla_{\mathbf{I}}G(\mathbf{I},\phi) \\ &= 2\pi i\Big(\sum_{\mathbf{l}}\nabla_{\mathbf{I}}H_l(\mathbf{I})e^{2\pi i\mathbf{l}\cdot\phi}\cdot\sum_{\mathbf{k}\neq 0}\mathbf{k}G_k(\mathbf{I})e^{2\pi i\mathbf{k}\cdot\phi} - \\ &\qquad \sum_{\mathbf{l}}\mathbf{l}\nabla_\phi H_l(\mathbf{I})e^{2\pi i\mathbf{l}\cdot\phi}\cdot\sum_{\mathbf{k}\neq 0}\nabla_{\mathbf{I}}G_k(\mathbf{I})e^{2\pi i\mathbf{k}\cdot\phi}\Big) \\ &= 2\pi i\sum_{\mathbf{l}}\sum_{\mathbf{k}\neq 0}[(\mathbf{k}\cdot\nabla_{\mathbf{I}}H_l(\mathbf{I}))G_k(\mathbf{I}) - \\ &\qquad (\mathbf{l}\cdot\nabla_{\mathbf{I}}G_k(\mathbf{I}))H_l(\mathbf{I})]e^{2\pi i(1+\mathbf{k})\cdot\phi} \\ &= 2\pi i\sum_{\mathbf{n}}\sum_{\mathbf{k}\neq 0}[(\mathbf{k}\cdot\nabla_{\mathbf{I}}H_{\mathbf{n}-\mathbf{k}}(\mathbf{I}))G_k(\mathbf{I}) - \\ &\qquad ((\mathbf{n}-\mathbf{k})\cdot\nabla_{\mathbf{I}}G_k(\mathbf{I}))H_{\mathbf{n}-\mathbf{k}}(\mathbf{I})]e^{2\pi i\mathbf{n}\cdot\phi} \end{aligned} \tag{16}$$

and so, our system of nonlinear PDEs is given by

$$\frac{\partial H_n}{\partial t} = 2\pi i\sum_{\mathbf{k}\neq 0}[(\mathbf{k}\cdot\nabla_{\mathbf{I}}H_{\mathbf{n}-\mathbf{k}})G_k - ((\mathbf{n}-\mathbf{k})\cdot\nabla_{\mathbf{I}}G_k)H_{\mathbf{n}-\mathbf{k}}) \tag{17}$$

This is the basic evolution which we are seeking. Note that the

dynamics occurs at constant **I**, and so, as with the CGM and CHM methods, **I** is a fixed parameter set at the beginning of the program, making this method suitable for EBK quantization. Before discussing how we choose our $\{G_k\}$, we will first impose some constraints on the infinitesimal generating functions.

The first constraint that we impose comes from the fact that our Hamiltonian must remain real during the evolution. Therefore, we must have $H = \bar{H}$. But $H = \sum_{\mathbf{n}} H_n e^{2\pi i \mathbf{n}\cdot\phi} = \sum_{\mathbf{n}} H_{-n} e^{-2\pi i \mathbf{n}\cdot\phi}$, and so $\bar{H} = \sum_{\mathbf{n}} \bar{H}_n e^{-2\pi i \mathbf{n}\cdot\phi}$, from which we deduce that $\bar{H}_n = H_{-n}$. To maintain this property, we must have $\partial\bar{H}_n/\partial t = \partial\bar{H}_{-n}/\partial t$. Now,

$$\begin{aligned}\frac{\partial \bar{H}_n}{\partial t} &= -2\pi i \sum_{\mathbf{k}\neq 0} [(\mathbf{k}\cdot\nabla_{\mathbf{I}}\bar{H}_{\mathbf{n}-\mathbf{k}})\bar{G}_k - ((\mathbf{n}-\mathbf{k})\cdot\nabla_{\mathbf{I}}\bar{G}_k)\bar{H}_{\mathbf{n}-\mathbf{k}}] \\ &= 2\pi i \sum_{\mathbf{k}\neq 0} [(-\mathbf{k}\cdot\nabla_{\mathbf{I}}H_{\mathbf{k}-\mathbf{n}})\bar{G}_k - ((\mathbf{k}-\mathbf{n})\cdot\nabla_{\mathbf{I}}\bar{G}_k)\bar{H}_{\mathbf{k}-\mathbf{n}}] \\ &= 2\pi i \sum_{\mathbf{k}\neq 0} [(\mathbf{k}\cdot\nabla_{\mathbf{I}}H_{-\mathbf{n}-\mathbf{k}})\bar{G}_{-k} - ((-\mathbf{n}-\mathbf{k})\cdot\nabla_{\mathbf{I}}\bar{G}_{-k})H_{-\mathbf{n}-\mathbf{k}}]\end{aligned} \tag{18}$$

We also have

$$\frac{\partial H_{-n}}{\partial t} = 2\pi i \sum_{\mathbf{k}\neq 0} [(\mathbf{k}\cdot\nabla_{\mathbf{I}}H_{-\mathbf{n}-\mathbf{k}})G_k - ((-\mathbf{n}-\mathbf{k})\cdot\nabla_{\mathbf{I}}G_k)H_{-\mathbf{n}-\mathbf{k}}] \tag{19}$$

and so we see that to have equality between the two expressions we must take $\bar{G}_k = G_{-k}$, i.e., our generating functions must also be real.

The next constraint that we impose comes from the fact that we shall assume time-reversal invariance in this paper. Our torus quantization program will be used for problems related to the vibrational dynamics of polyatomic molecules. No magnetic field is present, and so time-reversal invariance holds for the Hamiltonians of these systems. Thus, our Fourier components H_n may be taken to be real, and we would like this property to hold throughout the evolution. Therefore, we want $\partial H_n/\partial t = \partial\bar{H}_n/\partial t = \partial H_{-n}/\partial t$. Using the fact that $H_{-n} = \bar{H}_n = H_n$ gives us that

$$\begin{aligned}\frac{\partial H_{-n}}{\partial t} &= 2\pi i \sum_{\mathbf{k}\neq 0} [(\mathbf{k}\cdot\nabla_{\mathbf{I}}H_{\mathbf{n}+\mathbf{k}})G_k + ((\mathbf{n}+\mathbf{k})\cdot\nabla_{\mathbf{I}}G_k)H_{\mathbf{n}+\mathbf{k}}] = \\ &\quad 2\pi i \sum_{\mathbf{k}\neq 0} [(\mathbf{k}\cdot\nabla_{\mathbf{I}}H_{\mathbf{n}-\mathbf{k}})(-G_{-k}) - ((\mathbf{n}-\mathbf{k})\cdot\nabla_{\mathbf{I}}(-G_{-k}))H_{\mathbf{n}-\mathbf{k}}]\end{aligned} \tag{20}$$

and so we must have $G_k = -G_{-k}$. Combined with the fact that $\bar{G}_k = G_{-k}$, we obtain $\bar{G}_k = -G_k = G_{-k}$. Thus, G_k must be purely imaginary, and so we can write $G_k = i\hat{G}_k$, where $\hat{G}_k$ is real. Since $-G_k = G_{-k}$, we must have $\hat{G}_{-k} = -\hat{G}_k$. Putting everything together, our system of PDEs becomes

$$\frac{\partial H_n}{\partial t} = -2\pi \sum_{\mathbf{k}\neq 0} [(\mathbf{k}\cdot\nabla_{\mathbf{I}}H_{\mathbf{n}-\mathbf{k}})\hat{G}_k - ((\mathbf{n}-\mathbf{k})\cdot\nabla_{\mathbf{I}}\hat{G}_k)H_{\mathbf{n}-\mathbf{k}}] \tag{21}$$

where the $\hat{G}_k$ are real and $\hat{G}_{-k} = -\hat{G}_k$. For simplicity of notation, we shall henceforth drop the hats from the G_k terms.

4.3. Choosing the G_k. We wish to choose our G_k in such a way as to decrease $|H_n|$, or equivalently, $H_n\bar{H}_n = H_n^2$. In the limit of a weak perturbation, all H_m, $\mathbf{m} \neq 0$ are small compared to H_0, and so $\partial H_n/\partial t \approx -2\pi(\mathbf{n}\cdot\nabla_{\mathbf{I}}H_0)G_n$. Therefore, $\partial H_n^2/\partial t \approx -4\pi H_n(\mathbf{n}\cdot\nabla_{\mathbf{I}}H_0)G_n$, hence in the weakly perturbed limit the gradient descent prescription for minimizing H_n^2 is to take $G_k = 4\pi(\mathbf{k}\cdot\nabla_{\mathbf{I}}H_0)H_k$. Note that G_k is real and satisfies $G_{-k} = -G_k$.

For stronger perturbations, this choice for the G_k does not coincide with the gradient descent values. However, one would expect that for perturbations that are not too strong (which is a reasonable assumption, since we want to remain in the quasi-integrable regime of phase space), the above choice of G_k should decrease the H_n^2. At the beginning of the evolution there will be a discrepancy between our choice for G_k and the actual gradient-descent values. If our G_k start decreasing the H_n^2 from the beginning, then our perturbative terms should gradually get smaller, so that our choice for the G_k should get better and better as the evolution proceeds. In summary, then, we take

$$G_k = 4\pi(\mathbf{k}\cdot\nabla_{\mathbf{I}}H_0)H_k \tag{22}$$

Notice that this choice for G_k eliminates the need to determine what terms in the Hamiltonian are to be considered resonances or not. The closer an integer vector **k** corresponds to a resonance, the smaller the corresponding G_k, and so the less that term in the Hamiltonian is affected by the evolution. Thus, this evolution scheme evolves the Fourier components of the Hamiltonian in such a way that the nonresonant behavior is incorporated into an integrable Hamiltonian, leaving only the resonant terms to couple the resulting IRR basis.

It should also be noted that this choice for G_k leads to first-order perturbation theory in the limit of small perturbations. This is shown in Appendix B.

5. Numerical Implementation of the PDE

5.1. Overall Structure of the Algorithm. We begin by choosing our basis of quantum number vectors $\{|\mathbf{n}\rangle\}$. With this basis we generate our Hamiltonian matrix via the semiclassical prescription $\langle\mathbf{m}|\bar{H}|\mathbf{n}\rangle = H_{\mathbf{m}-\mathbf{n}}(\mathbf{I}_{\mathbf{m}}+\mathbf{I}_{\mathbf{n}}/2)$, as described in eq 12. We thus construct a list $\mathbf{I}_{\mathbf{r}}$ of the actions $\mathbf{I}_{\mathbf{m}}+\mathbf{I}_{\mathbf{n}}/2$ involved in our semiclassical matrix. It is on this discrete set of actions that we will apply our gradient-descent algorithm. At the end of the program, the $H_n(\mathbf{I}_{\mathbf{r}})$ will have been changed to their final values. For each $\mathbf{I}_{\mathbf{r}}$ we also store all the associated $\mathbf{s} \equiv \mathbf{m} - \mathbf{n}$. The final values of $H_{\mathbf{s}}(\mathbf{I}_{\mathbf{r}})$ are then placed into their appropriate positions in the semiclassical matrix, thereby giving us our final Hamiltonian matrix, which we then diagonalize to determine the semiclassical spectrum.

5.2. Dynamics at a Given Action. We now turn to the dynamics at a given action vector, which we denote by $\mathbf{I}_0$. Note that $G_k = 4\pi(\mathbf{k}\cdot\nabla_{\mathbf{I}}H_0)H_k \Rightarrow \nabla_{\mathbf{I}}G_k = 4\pi(\mathbf{k}\cdot\nabla_{\mathbf{I}}H_0)\nabla_{\mathbf{I}}H_k + 4\pi(\mathbf{k}\cdot D\nabla_{\mathbf{I}}H_0)H_k$. Now, the systems we study are harmonic-oscillator Hamiltonians which are perturbed by some anharmonic terms (as mentioned before, the target systems of this algorithm are model vibrational Hamiltonians of polyatomic molecules). For a purely harmonic system, $D\nabla_{\mathbf{I}}H_0 = 0$, such a small perturbation gives us that $(\mathbf{k}\cdot D\nabla_{\mathbf{I}}H_0)H_k$ is at most second-order in the perturbation strength. Thus, the dominant term in $\nabla_{\mathbf{I}}G_k$ is $4\pi(\mathbf{k}\cdot\nabla_{\mathbf{I}}H_0)\nabla_{\mathbf{I}}H_k$. Using this value in our evolution equation suggests we solve the PDE as follows:

$$\begin{aligned}\frac{\partial H_n}{\partial t} = -8\pi^2 \sum_{\mathbf{k}\neq 0} &[(\mathbf{k}\cdot\nabla_{\mathbf{I}}H_{\mathbf{n}-\mathbf{k}})H_k - \\ &((\mathbf{n}-\mathbf{k})\cdot\nabla_{\mathbf{I}}H_k)H_{\mathbf{n}-\mathbf{k}}](\mathbf{k}\cdot\nabla_{\mathbf{I}}H_0)\end{aligned} \tag{23}$$

Although this PDE is not the exact one we wish to solve, we expect that for small perturbations it should be sufficiently accurate. As we shall see with the model systems studied in

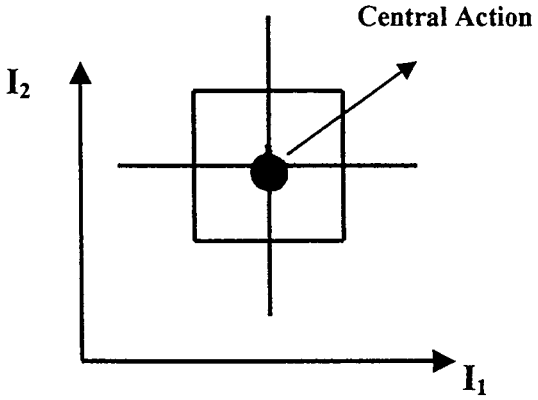

Figure 1. Diagram of an action grid with $D = 2$ and GDSZ = 2.

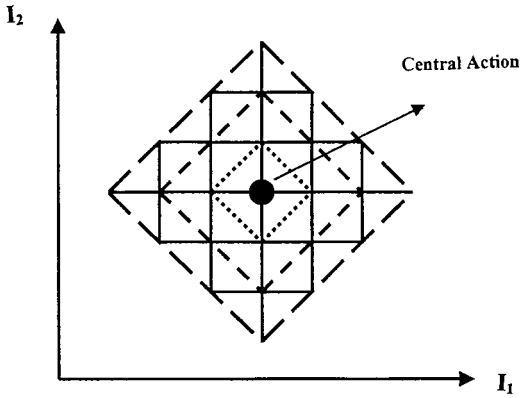

Figure 2. Collapsing boundary upon successive iterations of our PDE.

this paper, this approximate PDE is sufficiently accurate to give us the semiclassical spectrum.

We solve this system of PDEs on a grid of actions about the central action $\mathbf{I}_0$ where our grid consists of all actions $\mathbf{I}_k = \mathbf{I}_0 + DX\mathbf{k}$, with $\mathbf{k} = (k_1,...,k_D)$ satisfying $|k_1| + ... + |k_D| \leq$ GDSZ. Let us denote this set of grid points as $\Omega(\mathbf{I}_0, \text{GDSZ})$. GDSZ and DX are user-input parameters. A sample grid with $D = 2$ and GDSZ = 2 is presented in Figure 1.

At the beginning of evolution, we first compute all of the H_k on all the grid points about the action $\mathbf{I}_0$. We cannot compute H_k for all vectors $\mathbf{k}$, so we make a user-input cutoff MAXK. Thus, we only track those $\mathbf{k}$ for which $|k_1| + ... + |k_D| \leq$ MAXK. All other H_k are set to 0 throughout the evolution. Furthermore, to eliminate tracking negligible fast terms we introduce a resonance half-width, RHW, and further restrict ourselves to those $\mathbf{k}$ for which $|\mathbf{k}\cdot\omega| <$ RHW, where ω is the vector of the zeroth-order harmonic frequencies.

The initial H_k are computed analytically. We start with an initial, zeroth-order action-angle basis of harmonic oscillators. Our Hamiltonian is

$$H(\mathbf{x},\mathbf{p}) = \frac{\mathbf{p}^2}{2} + \frac{1}{2}(\omega_1^2 x_1^2 + ... + \omega_D^2 x_D^2) + \sum_{N=3}^{M} \sum_{n_1+...+n_D=N} \frac{1}{n_1!...n_D!} \alpha_{(n_1,...,n_D)} x_1^{n_1}...x_D^{n_D} \quad (24)$$

We take all our masses to be 1, because in a polyatomic molecule, a normal-mode analysis involves a transformation to a system of mass-scaled coordinates in which all of the masses become 1. The transformation to harmonic-oscillator action-angle coordinates is then accomplished via

$$x_k = \sqrt{\frac{I_k}{\pi\omega_k}} \cos 2\pi\theta_k \quad (25)$$

$$p_k = -\sqrt{\frac{\omega_k I_k}{\pi}} \sin 2\pi\theta_k \quad (26)$$

Once the H_k have been determined, we compute all gradients using centered differences, giving us an $O(DX^2)$ accurate estimate. We then propagate forward by one time step of length DT, which is also user-specified. (This propagation step is described in Appendix A.1.) Note that we cannot evaluate $\nabla_I H_k$ at the boundary of our grid. Thus, we cannot change the values at the boundary points. However, all grid points in $\Omega(\mathbf{I}_0, \text{GDSZ} - 1)$ have been propagated correctly, and so after the first iteration step we continue propagation only at those grid points.

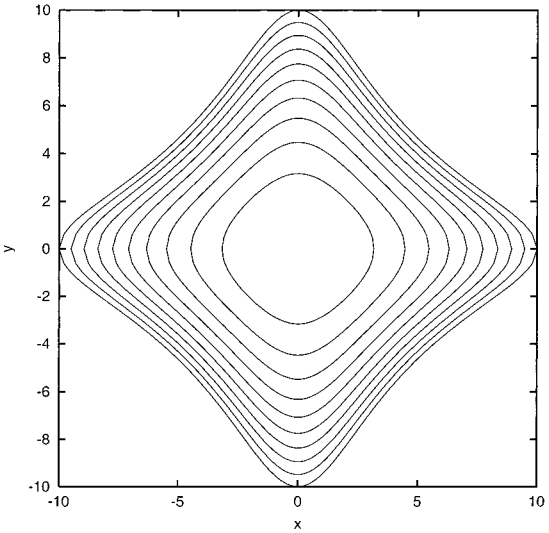

Figure 3. Contour plot of the Pullen−Edmonds potential $1/2\ (x^2 + y^2) + 0.05x^2y^2$ for $E = 5, 10, ..., 50$.

Note that after the second iteration we continue propagating only on $\Omega(\mathbf{I}_0, \text{GDSZ} - 2)$. Continuing this process, we get that after the ith iteration we continue propagating only on $\Omega(\mathbf{I}_0, \text{GDSZ} - i)$, and so the total number of iterations cannot exceed GDSZ. This scheme avoids the need for imposing artificial boundary conditions on our system. Rather, around each $\mathbf{I}_0$ we have a collapsing boundary, inside of which the H_k's are propagated correctly at each time step (see Figure 2). Furthermore, because we care only about the values of the H_k at $\mathbf{I}_0$, we may as well set the number of iterations and GDSZ to be equal. For a desired number of iterations, this gives the minimum value of GDSZ possible, which increases the algorithm's speed and minimizes memory requirements.

6. Numerical Examples

6.1. Two Degrees of Freedom. We first demonstrate our method using the Pullen−Edmonds Hamiltonian[5]

$$H = \frac{p_x^2 + p_y^2}{2} + \frac{1}{2}(\omega_x^2 x^2 + \omega_y^2 y^2) + \epsilon x^2 y^2 \quad (27)$$

where we set $\omega_x = \omega_y = 1$ and $\epsilon = 0.05$. This is the system studied by Carioli et al.[1] in illustrating the CHM method, which is why we shall also use it to illustrate our method, so that there is a frame of reference for comparison.

In Figure 3 we give a contour plot of this Hamiltonian at energies $E = 5, 10, ... 50$. This system has four symmetry axes,

TABLE 1: Two-Degree-of-Freedom Example[a]

state	QM	SC	0 iterations	2 iterations
37	9.1548	9.1482	9.1731	9.1506
38	9.1577	9.1514	9.1812	9.1538
39	9.3806	9.3747	9.4199	9.3747
40	9.4265	9.4219	9.5045	9.4224
41	9.5166	9.5150	9.5904	9.5133
42	9.6859	9.6876	9.8438	9.6861
43	9.6987	9.6988	9.8519	9.6983
44	10.0129	10.0163	10.2736	10.0163
45	10.0133	10.0169	10.2740	10.0167

[a] Energies of states 37 to 45 obtained by various methods. Column 2: Exact quantum-mechanical. Column 3: Exact semiclassical. Column 4: 9×9 block diagonalization in the harmonic oscillator torus basis. Column 5: 9×9 block diagonalization in the IRR basis.

giving rise to four modes of oscillation: Two "local" modes, corresponding to oscillation along the x and y axes, and two "normal" modes, corresponding to oscillation along the lines $y = \pm x$. There is strong dynamical tunneling between the "local" modes in the quasi-integrable regime that leads to a quantum-mechanical breaking of the degeneracy in the spectrum.

Following Carioli et al. we looked at those quantum states (n_1,n_2) satisfying $n_1 + n_2 = 8$. This gives us 9-fold degenerate states with zeroth-order energy $E = 9$. The system is in the quasi-integrable regime at this energy. If we count up from the ground-state (0, 0), then we find that these nine states are states 37 to 45 of our system.

Upon introducing the anharmonic coupling term to our system, the degeneracy of these states is broken, giving the quantum-mechanical energies listed in the second column of Table 1. These energies were obtained by diagonalizing all states from the ground state up to a total of sixteen quanta. Using the semiclassical coupling prescription given in eq 12, we also found the corresponding semiclassical energies using the harmonic-oscillator tori as our basis. As with the quantum energies, these energies were also determined by diagonalizing all states up to a total of sixteen quanta. The energies obtained were the same energies obtained by Carioli et al. using the IRR approach. These energies are in the third column of Table 1.

We next diagonalized only the 9×9 block of our 9-fold degenerate states using the harmonic-oscillator tori as our semiclassical basis. The results are listed in the fourth column of Table 1. Note the significant discrepancy between these energies and the exact semiclassical energies. (By exact semiclassical energies we mean the energies obtained using the same harmonic basis used to obtain the quantum energies, but using the semiclassical couplings instead of the quantum couplings.) We applied our GDA method to these nine degenerate states, using $DT = 0.0007$, $DX = 0.1$, MAXK $= 8$, RHW $= 8.1$, and iterating twice. The results are listed in the fifth column of Table 1. Note that the discrepancy with the exact semiclassical energies has been drastically reduced, by at least 90% in all cases, and by over 99% in most. Thus, while our method is not quite as accurate as the CHM method, it is nearly so. Furthermore, the disrepancy between the two methods is well within the discrepancy between the exact semiclassical and exact quantum energies.

Carioli et al. also performed a sweep of ω_x from 0.99 to 1.01 to look at the avoided crossing between states 39 and 40. In Figure 4(a) we show the semiclassical energy curves for the two states, along with the curves obtained by diagonalizing the 9×9 block using the harmonic-oscillator tori as our basis. In Figure 4b we also show the semiclassical energy curves for the two states, along with the curves obtained by applying our gradient descent method to our zeroth-order 9-fold degenerate basis (with the same program parameters as before). Note that the discrepancy present in Figure 4a has been eliminated. To be sure, the match is not exact, but the differences cannot be seen at the resolution level of the plot.

6.2. Four Degrees of Freedom. To demonstrate the speed of our method, we used it to determine the EBK spectrum of the four-dimensional Hamiltonian,

$$H = \frac{p_x^2 + p_y^2 + p_z^2 + p_w^2}{2} + \frac{1}{2}(x^2 + y^2 + z^2 + w^2) + 0.05(0.97x^2y^2 + 0.98x^2z^2 + 0.99x^2w^2 + 1.01y^2z^2 + 1.02y^2w^2 + 1.03z^2w^2) \quad (28)$$

We looked at those quantum states (n_1, n_2, n_3, n_4) satisfying $n_1 + n_2 + n_3 + n_4 = 8$. This gave us 165-fold degenerate states with a zeroth-order energy of $E = 10$. Counting up from the ground-state gives us that these are states 331 to 495 of our system.

The quantum and exact semiclassical energies of these states were obtained by diagonalizing all states up to a total of sixteen quanta. The results are listed in the second and third columns, respectively, of Table 2. Note that we do not list all 165 energies, but rather only a representative sample. As with the two-dimensional case, we also diagonalized the 165×165 block of our degenerate states, using the zeroth-order harmonic oscillator tori as our semiclassical basis. This gives us the energies in the fourth column of Table 2. Finally, we applied our algorithm to this basis using the parameters $DT = 0.0007$, $DX = 0.1$, MAXK $= 8$, RHW $= 4.1$, and iterating twice. The results are listed in the fifth column of Table 2.

The average initial discrepancy between our IRR energies, given in the fourth column, and the exact semiclassical energies was 3.0%. The final discrepancy was 0.2%. Thus, our algorithm, in two iterations, reduced the initial error in the energies by an average of 93.3% and by at least 80% for all our energies. There are four "anomalous" energies near the top of the band with significantly greater error than the other energies, but even for these energies the final error is around 1%. At this point it should be noted that our perturbation might be a little large for our PDE (which neglected the $D\nabla_{\mathbf{I}}H_0$ term), because the initial energy gap that needed to be closed was on average several times larger than the initial energy gap in our two-dimensional example.

6.3. Six Degrees of Freedom. We conclude this section by looking at a six-degree-of-freedom example. As with the four-dimensional example, the Hamiltonian we chose was a generalization of the Pullen−Edmonds system. We took

$$H = \frac{1}{2}\sum_{k=1}^{6}(x_k^2 + p_k^2) + 0.05(0.93x_1^2x_2^2 + 0.94x_1^2x_3^2 + 0.95x_2^2x_3^2 + 0.96x_1^2x_4^2 + 0.97x_2^2x_4^2 + 0.98x_3^2x_4^2 + 0.99x_1^2x_5^2 + 1.00x_2^2x_5^2 + 1.01x_3^2x_5^2 + 1.02x_4^2x_5^2 + 1.03x_1^2x_6^2 + 1.04x_2^2x_6^2 + 1.05x_3^2x_6^2 + 1.06x_4^2x_6^2 + 1.07x_5^2x_6^2) \quad (29)$$

We initially tried to obtain the exact quantum and semiclassical energies of the states with a total of 8 quanta in the unperturbed limit. While applying our method to this basis would not have been a problem, we would not have been able to generate the exact quantum and semiclassical energies required for comparison. As with the two- and four-dimensional cases, we would

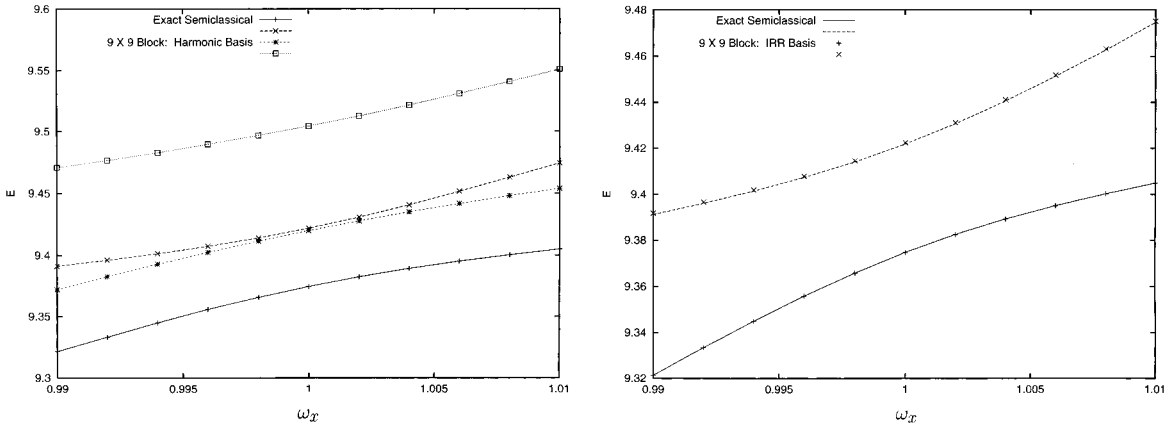

Figure 4. (a) Semiclassical avoided crossing between states 39 and 40 as a function of ω_x. The curves here are the exact semiclassical energies and the energies obtained by diagonalizing the 9 × 9 block in the harmonic oscillator torus basis. (b) Semiclassical avoided crossing between states 39 and 40 as a function of ω_x. The curves here are the exact semiclassical energies and the energies obtained by diagonalizing the 9 × 9 block in the IRR torus basis. The IRR basis was generated using the gradient-descent algorithm.

TABLE 2: Four-Degree-of-Freedom Example[a]

state	QM	SC	0 iterations	2 iterations
331	10.4846	10.4658	10.5753	10.4821
332	10.4877	10.4688	10.5812	10.4853
333	10.4902	10.4712	10.5846	10.4877
334	10.4972	10.4777	10.5936	10.4942
335	10.7116	10.6961	10.8517	10.7137
336	10.7147	10.6992	10.8557	10.7167
337	10.7179	10.7023	10.8598	10.7198
338	10.7238	10.7081	10.8675	10.7256
339	10.7271	10.7114	10.8717	10.7288
340	10.7304	10.7146	10.8759	10.7320
341	10.7426	10.7268	10.9048	10.7455
342	10.7460	10.7302	10.9095	10.7488
343	10.7493	10.7334	10.9142	10.7520
344	10.7564	10.7403	10.9238	10.7587
345	10.7596	10.7435	10.9283	10.7618
346	10.7628	10.7466	10.9329	10.7648
347	10.8320	10.8198	10.9943	10.8375
348	10.8355	10.8231	10.9980	10.8407
349	10.8530	10.8418	11.0288	10.8591
350	10.8564	10.8450	11.0323	10.8623
480	11.5308	11.5132	12.0430	11.5416
481	11.5323	11.5156	12.0476	11.5444
482	11.5339	11.5230	12.0525	11.5471
483	11.5350	11.5314	12.0580	11.5503
484	11.5369	11.5321	12.0623	11.5527
485	11.5376	11.5345	12.0633	11.5527
486	11.5401	11.5375	12.0660	11.5548
487	11.5402	11.5409	12.0718	11.5576
488	11.5427	11.5435	12.2613	11.6688
489	11.5450	11.5449	12.2805	11.6791
490	11.5455	11.5458	12.2819	11.6798
491	11.5456	11.5503	12.2834	11.6806
492	11.6628	11.6669	12.2850	11.6815
493	11.6692	11.6793	12.2865	11.6823
494	11.6699	11.6801	12.2878	11.6830
495	11.6707	11.6810	12.3028	11.6911

[a] A sample of energies of states 331 to 495 obtained by various methods. Column 2: Exact quantum-mechanical. Column 3: Exact semiclassical. Column 4: 165 × 165 block diagonalization in the harmonic oscillator torus basis. Column 5: 165 × 165 block diagonalization in the IRR basis.

have had to diagonalize all states up to a total of sixteen quanta to get the higher-order accuracy desired. The resulting basis was simply too large for our computer to handle, and so we had to retreat to a more manageable example. We thus looked at those quantum states (n_1, n_2, n_3, n_4, n_5, n_6) satisfying $n_1 + n_2 + n_3 + n_4 + n_5 + n_6 = 4$, giving us 126 degenerate states with a zeroth-order energy of $E = 7$. Counting from the ground-state as before, we get that these are states 85 to 210 of our system.

The quantum and exact semiclassical energies were then obtained by diagonalizing all states up to a total of eight quanta. The results are listed in the second and third columns, respectively, of Table 3. We do not list all 126 energies, but rather only a representative sample. Proceeding as before, we then diagonalized only the 126 × 126 block of degenerate states, using the zeroth-order harmonic oscillator tori as our basis. The results are given in the fourth column of Table 3. Finally, we applied our gradient-descent algorithm to this degenerate basis. Using MAXK = 8 gave us so many resonances and fast terms that the run-time was prohibitively slow. So, we sacrificed accuracy for speed and used the parameters $DT = 0.0007$, $DX = 0.1$, MAXK = 4, RHW = 4.1, and iterated twice. The results are given in the fifth column of Table 3. Notice that although we significantly reduced the number of available resonances and fast terms, we still managed to cut the initial energy discrepancy from an average of 2.3% to an average of 0.4%. This corresponds to an average reduction in the initial error by 83.3%, with a minimum reduction of 78.7% and a maximum reduction of 90.4%.

6.4. Discussion. Notice that in all our examples, just using the degenerate basis of harmonic-oscillator tori did not give us a good estimate of the semiclassical energies. It was necessary to diagonalize all states within a much wider energy band to do so. Although harmonic oscillators are probably the easiest basis states to use for the potentials of interest to us in this paper, it is generally a mistake to attach a mechanism to the energy flow associated with this basis. Stuchebrukhov and Marcus,[7] using a harmonic-oscillator basis to study 0.01−0.1 cm^{-1} energy splittings in a polyatomic molecule with 42 vibrational degrees of freedom, had to diagonalize all states within an energy band of 10 cm^{-1} or more. They invoked the concept of a "superexchange" mechanism, whereby energy flow between nearly degenerate states, but distantly separated in the quantum number space, occurred via energy flow between states closer to each other in the quantum number space but with a larger energy gap between them. This "superexchange" mechanism is a basis-dependent notion, however, as is most simply illustrated by our two-degree-of-freedom example. To obtain the semiclassical energies of states 37 to 45, with a total energy range <1, we had to diagonalize a much larger basis of 153 states with a total energy range of >20. We could also invoke a "superexchange" mechanism for this energy flow. Indeed,

TABLE 3: Six-Degree-of-Freedom Example[a]

state	QM	SC	0 iterations	2 iterations
85	7.5094	7.4947	7.6006	7.5181
86	7.5245	7.5108	7.6220	7.5347
87	7.5272	7.5133	7.6254	7.5374
88	7.5307	7.5167	7.6299	7.5408
89	7.5363	7.5220	7.6371	7.5464
90	7.5454	7.5305	7.6485	7.5552
91	7.6178	7.6063	7.7413	7.6328
92	7.6199	7.6083	7.7440	7.6349
93	7.6220	7.6104	7.7468	7.6370
94	7.6232	7.6116	7.7484	7.6383
95	7.6253	7.6137	7.7512	7.6404
96	7.6274	7.6157	7.7539	7.6425
97	7.6286	7.6169	7.7554	7.6436
98	7.6307	7.6189	7.7582	7.6458
99	7.6328	7.6210	7.7610	7.6479
100	7.6356	7.6237	7.7648	7.6507
190	7.8028	7.7952	7.9992	7.8256
191	7.8045	7.7959	8.0010	7.8265
192	7.8052	7.7976	8.0020	7.8272
193	7.8069	7.7979	8.0035	7.8289
194	7.8086	7.7993	8.0073	7.8307
195	7.8581	7.8608	8.0973	7.8892
196	7.8598	7.8625	8.0998	7.8908
197	7.8615	7.8642	8.1023	7.8925
198	7.8624	7.8651	8.1036	7.8934
199	7.8640	7.8667	8.1061	7.8950
200	7.8657	7.8684	8.1086	7.8967
201	7.8664	7.8691	8.1096	7.8974
202	7.8680	7.8707	8.1121	7.8990
203	7.8697	7.8724	8.1146	7.9006
204	7.8719	7.8746	8.1179	7.9028
205	7.8722	7.8750	8.1186	7.9032
206	7.8739	7.8766	8.1211	7.9049
207	7.8756	7.8782	8.1235	7.9065
208	7.8778	7.8804	8.1268	7.9087
209	7.8811	7.8837	8.1319	7.9120
210	7.9164	7.9295	8.1999	7.9556

[a] A sample of energies of states 85 to 210 obtained by various methods. Column 2: Exact quantum-mechanical. Column 3: Exact semiclassical. Column 4: 126 × 126 block diagonalization in the harmonic oscillator torus basis. Column 5: 126 × 126 block diagonalization in the IRR basis.

shrinking our basis did give a small change in the energies (though only in the last one or two decimal places), so that one could argue that our perturbation is sufficiently strong to allow for such a mechanism. However, as is clear by applying our GDA method, a more accurate explanation is that while a superexchange mechanism is required to account for energy flow in the harmonic basis, there exists a basis obtainable from the underlying classical dynamics of the system, namely the IRR tori, in which the superexchange mechanism need not be invoked. Using the IRR tori we were able to obtain our nine semiclassical energies using a much smaller basis, which also lies within the energy range of our semiclassical spectrum. The "superexchange" mechanism is thus an artifact, coming from the fact that our zeroth-order basis of harmonic-oscillators is not the optimal basis of IRR tori.

Carioli et al. made one additional plot in their paper, in which they applied their CHM method in the chaotic regime, with $E = 50$. To obtain convergence of their method, they had to also include the fast terms arising from the vector $\mathbf{s} = (1,1)$. The IRR representation of the Hamiltonian was no longer block diagonal, though the coupling structure was still simplified somewhat. For this reason, we decided to forego our own study at $E = 50$. At best, our algorithm would simplify the coupling structure as well, so that a smaller basis would be required to obtain the semiclassical spectrum. In the chaotic regime, however, semiclassical quantization no longer occurs only on the invariant tori (due to ergodic regions of phase space of area significantly larger than $(2\pi\hbar)^D$), so that the IRR basis is no longer optimal. Another way of looking at this is that because our matrix is no longer block diagonal (though with a simplified coupling structure), we have to invoke the "superexchange" mechanism in order to account for the observed energies. At this point, we may as well use harmonic oscillators.

In the end, the use of invariant tori as a semiclassical basis for quantum calculations is most useful at relatively low energy, where the dynamics is quasi-integrable. It is in this regime that the IRR basis is expected to be most physically motivatived, and consequently leads to a significantly smaller basis, as well as giving physical insight.

7. Conclusions and Future Research

In this paper we presented an alternative approach to the CHM method for finding the IRR basis of a Hamiltonian system. Our approach is essentially a gradient-descent approach that continuously deforms our initial action-angle basis (taken to be harmonic oscillators) into an optimal basis of tori in which the angular dependence of the Hamiltonian is minimized. The advantage of the gradient-descent approach is that formally it does not distinguish between resonances and fast terms, so that all potential terms are evolved in a uniform fashion and reduced as much as possible. The CHM method, on the other hand, requires an a priori decision as to which terms are to be treated as resonances and which are going to be incorporated into creating the final tori. In the case of near-resonances this distinction is blurred and depends on the strength of the perturbation. In the chaotic regime, even fast terms may need to be treated as resonances. Although no speed comparisons were made, we believe that our method is also faster, since we do not have to evaluate any integrals or invert the angle map. Thus, our method can be used to study higher dimensional systems (up to $D = 6$ and maybe even higher).

Like the CHM method, our method, as currently implemented, assumes a small perturbation on a zeroth-order integrable Hamiltonian. Convergence is fast, requiring only two iterations in the examples studied in this paper. One approach to allow for stronger perturbations is to include the $(\mathbf{k}\cdot D\nabla_{\mathbf{I}}H_0)H_k$ term arising from our choice of G_k. The problem with this is that using our collapsing boundary method we would have to decrease GDSZ by 2 at each iteration step. If we wish to apply our method to higher-dimensional systems, this would greatly increase computation time, because two iterations would require a GDSZ of 4 as opposed to the current requirement of 2. As mentioned before, the systems of interest to us are Hamiltonians modeling the vibrational energy flow within polyatomic molecules. Because we wish to remain in the quasi-integrable regime, our Hamiltonians are taken to be harmonic plus some small anharmonic perturbation. Thus, including the term involving $D\nabla_{\mathbf{I}}H_0$ simply adds run time without any significant gains in accuracy for the types of systems of interest to us.

For more general Hamiltonians, a PDE approach may still be desirable, and yet our choice for G_k and our approximate PDE given in eq 23 may not be sufficient to obtain the IRR basis. Even if our current choice for the G_k is sufficient, we may find that a different choice leads to a more stable and accurate implementation of our PDE. In any case, one would have to retreat to eq 21 or even eq 17 (in the case where time-reversal invariance no longer holds) and formulate a different scheme for choosing the G_k. At this point it should be noted that the PDE approach may be the simplest and fastest overall

method for finding invariant tori, because it does not require the evaluation of any integrals or the numerical inversion of nonlinear functions.

Our future goal is to determine the structure of the matrices in the IRR basis. The greatest advantage of the IRR representation is that it incorporates much of the classical mechanics into the invariant tori, thereby making possible the isolation of residual quantum effects such as dynamical tunneling. An understanding of the couplings between the IRR tori will reveal how the tunnel couplings behave. This could in turn be used to understand phenomena such as localization of the tunneling, or if the perturbation is sufficiently strong, ergodicity over the energy hypersurface due to dynamical tunneling.

It has been mentioned in this paper that in the quasi-integrable regime, the couplings between the IRR tori correspond to dynamical tunneling in the semiclassical limit. Because the presence of resonances prevents the elimination of the IRR couplings $H_{\mathbf{m}-\mathbf{n}}$, it has been argued in ref 4 that it is the formation of resonance zones in the phase space that facilitates the tunneling. In a Poincare surface of section, the phase space surrounding a hyperbolic fixed point in the resonance zone looks much like the phase space for the one-dimensional above-barrier reflection problem,[4,11,13] which is a prime example of dynamical tunneling.

Classically, however, in 3 or more dimensions, Arnol'd diffusion can cause energy transport between the tori. A trajectory can travel along the Arnol'd web in the chaotic interstices between the tori, and may very well be ergodic over the energy hypersurface. Thus, in higher dimensions, a numerical study to determine whether the IRR couplings are primarily due to tunneling or to Arnol'd diffusion is necessary. The general consensus is that Arnol'd diffusion is slow and localizes quantum-mechanically.[4,12] A numerical study of this phenomenon is still warranted before making the claim with certainty that the IRR tori are coupled by dynamical tunneling.

Before concluding, it seems appropriate to briefly discuss the utility of the IRR approach in general, and the PDE implementation of it in particular, as a numerical method for quantum calculations. After all, it is usually easier and faster to use a convenient zeroth-order basis and simply diagonalize a large basis set. The PDE method is cumbersome by comparison, requiring more sophisticated mathematical and numerical machinery.

As the dimensionality of a system increases, the basis set required for a direct zeroth-order diagonalization could be too large for the computer to handle. As mentioned in section 6.3, we already encountered this problem in our numerical tests. The IRR approach can significantly reduce the size of the basis required to obtain the desired energies, to a point where this basis can easily be stored and diagonalized on the computer. Thus, while it is slower than direct diagonalization, this approach may be useful as a numerical method in cases where the required zeroth-order basis set size is simply too large for the computer to handle. The IRR approach has the additional advantage that the reduced basis is more physically motivated than the zeroth-order basis, because the IRR basis is extracted from the underlying classical dynamics of the system.

Acknowledgment. This research has been supported by NSF Grant CHE 0073544, and by an NSF Graduate Research Fellowship. The authors are deeply grateful to Bill Miller for leading the way into the semiclassical domain. Bill's work and friendship have shaped E.J.H.'s scientific career.

Appendix A. Numerical Details

In this appendix we give some additional numerical details regarding our implementation of the GDA method. The additional information provided here should make the results presented in this paper completely reproducible.

A.1. Numerically Stable Propagation. In this section we describe how we numerically integrate our PDE one time step forward. First of all, it should be noted that because we are considering all terms of the form $\mathbf{k}\cdot\nabla_{\mathbf{I}}H_0$, we are simultaneously evolving potential terms corresponding to resonances and fast terms. Thus, there is a variety of time scales in our system, so that stiffness becomes a problem. One way around this is to employ an implicit integration scheme to achieve stability, but we have a different method that takes advantage of the fact that our perturbation is small.

The first-order approximation to our evolution equation was shown to be $\partial H_n/\partial t = -8\pi^2(\mathbf{n}\cdot\nabla_{\mathbf{I}}H_0)^2H_n$, giving $H_n(\mathbf{I},t+\tau) = H_n(\mathbf{I},t)e^{-8\pi^2(\mathbf{n}\cdot\nabla_{\mathbf{I}}H_0)^2\tau}$. Therefore, for small τ we may write

$$\frac{\partial H_n(\mathbf{I},t+\tau)}{\partial\tau} = -8\pi^2\sum_{\mathbf{k}\neq 0}[(\mathbf{k}\cdot\nabla_{\mathbf{I}}H_{\mathbf{n}-\mathbf{k}}(\mathbf{I},t))H_k(\mathbf{I},t) - ((\mathbf{n}-\mathbf{k})\cdot\nabla_{\mathbf{I}}H_k(\mathbf{I},t))H_{\mathbf{n}-\mathbf{k}}(\mathbf{I},t)] \times (\mathbf{k}\cdot\nabla_{\mathbf{I}}H_0)e^{-8\pi^2((\mathbf{k}\cdot\nabla_{\mathbf{I}}H_0)^2+((\mathbf{n}-\mathbf{k})\cdot\nabla_{\mathbf{I}}H_0)^2)\tau} \tag{A1}$$

so integrating τ from 0 to DT gives

$$H_n(\mathbf{I},t+DT) = H_n(\mathbf{I},t) - \sum_{\mathbf{k}\neq 0}(1-e^{-8\pi^2((\mathbf{k}\cdot\nabla_{\mathbf{I}}H_0)^2+((\mathbf{n}-\mathbf{k})\cdot\nabla_{\mathbf{I}}H_0)^2)DT})(\mathbf{k}\cdot\nabla_{\mathbf{I}}H_0) \times \frac{(\mathbf{k}\cdot\nabla_{\mathbf{I}}H_{\mathbf{n}-\mathbf{k}}(\mathbf{I},t))H_k(\mathbf{I},t) - ((\mathbf{n}-\mathbf{k})\cdot\nabla_{\mathbf{I}}H_k(\mathbf{I},t))H_{\mathbf{n}-\mathbf{k}}(\mathbf{I},t)}{(\mathbf{k}\cdot\nabla_{\mathbf{I}}H_0)^2+((\mathbf{n}-\mathbf{k})\cdot\nabla_{\mathbf{I}}H_0)^2} \tag{A2}$$

Of course, if $\alpha \equiv (\mathbf{k}\cdot\nabla_{\mathbf{I}}H_0)^2 + ((\mathbf{n}-\mathbf{k})\cdot\nabla_{\mathbf{I}}H_0)^2$ is too close to 0, then the computer will give a floating exception error if we try to evaluate $1 - e^{-8\pi^2\alpha DT}/\alpha$ directly. We thus evaluate this term as follows: We define $x = 8\pi^2\alpha DT$, and rewrite our expression as $8\pi^2DT\ 1 - e^{-x}/x$. We then evaluate $1 - e^{-x}/x$ via its Taylor expansion, given by $\sum_{n=0}^{\infty}(-x)^n/(n+1)!$.

By expanding the exponential out to first-order, we see that this approach reduces to the ordinary one-step explicit Euler method for sufficiently small DT. However, the above method is superior to using an explicit Euler method because we can now take larger time steps that are more appropriate to the slow terms arising from resonances or near-resonances. These larger time steps do not lead to numerical instability, since the more nonresonant terms (corresponding to the shorter time scales requiring smaller time steps to maintain stability in the explicit Euler scheme) are attenuated by the exponential factor. In fact, since we want to kill off the nonresonant terms in any case, there is an optimum time step which kills off the nonresonant terms as much as possible without sacrificing accuracy.

It turns out that our propagation scheme is still not as stable as desired. This is remedied by propagating using the Lax method.[10] Let $(\hat{\mathbf{e}}_1,\ldots,\hat{\mathbf{e}}_D)$ denote the standard orthonormal basis of $\mathbf{R}^D$. At some $\mathbf{I}_k$ on our action grid, let $\mathbf{I}_k^{i\pm}$ denote $\mathbf{I}_k \pm DX\hat{\mathbf{e}}_i$. Then in eq A2 we replace $H_n(\mathbf{I}_k,t)$ with $\sum_{i=1}^{D}H_n(\mathbf{I}_k^{i+},t) + H_n(\mathbf{I}_k^{i-},t)/2D$. This trick adds a diffusive term to our propagation, which attenuates high-frequency components and therefore stabilizes our system if DT and DX are in an appropriate ratio. An explicit stability analysis was not performed on this system, so we do not know what the exact stability criterion is. We

simply found that employing a Lax method allowed us to choose a reasonable *DT* and *DX* to integrate our PDE numerically without getting a floating exception error after a few iterations.

It should be noted that in our actual code all of the actions were measured in units of 2π, meaning we set $I_i = \hbar(n_i + 1/2)$, as opposed to the convention that $I_i = h(n_i + 1/2) = 2\pi\hbar(n_i + 1/2)$. In creating our torus basis we stored the torus actions via their quantum numbers. Instead of multiplying by 2π to get a value consistent with the definition in eq 1, we simply left the actions in these "quantum number" units. We still implemented our PDE as written (i.e., with all the coefficients given in this paper). This implementation essentially amounts to a dilation of *DT* by $4\pi^2$. Thus, someone who wishes to reproduce the results presented below with an implementation of eq 23 using the definition of the actions given by eq 1 should increase all our *DT*'s by a factor of $4\pi^2$.

A.2. Numerical Issues. The main remaining problem with our implementation of the gradient-descent method is that it does not stop once we reach the IRR basis. In our two-dimensional case, using the parameters given above but iterating three times instead of two gives us a deviation from the semiclassical energies, especially at the higher end of the spectrum, where the method significantly underestimates the true semiclassical energies. After iterating five or six more times we get a floating exception, indicating that perhaps there are some numerical stability issues that have not been completely resolved and that lead to significant error already in the third iteration. Thus, the introduction of some kind of stopping term would be useful. The stopping criterion could be some kind of error term which, if the G_k drop below it, the program is stopped (such a criterion was employed in the CHM method to stop the Newton−Raphson iterations, though "overshooting" of the target was not a problem).

There are several reasons we have not included a stopping term at this point. First of all, as written, our gradient descent algorithm gives accurate results after only two iteration steps. Second, for higher dimensional systems, the number of resonances and fast terms increases rapidly. Because the size of the action grid also increases rapidly in higher dimensional systems, we would in any case never iterate more than 2 or 3 times in order to maintain a reasonable run time. Finally, a system that requires several iteration steps to give accurate results is typically more strongly perturbed than a system that requires fewer iteration steps. Such a more strongly perturbed system is less likely to be in the quasi-integrable regime of phase space, making a torus-quantization scheme less physically motivated in any case. Given these considerations, a stopping term becomes more of a feature that simply slows the algorithm down.

An alternative to a stopping term is to always iterate twice, but allow the computer to choose the optimum step size based on the initial perturbation. While we have not done this yet, we may decide to do so in the future.

Despite our reasoning, at some point it may become desirable to allow for more iterations. A more careful analysis of our PDE will be required to determine the cause of the inaccuracy at higher iterations. If it is due to numerical instability, then a more sophisticated approach than our current one may be required to better stabilize our evolution. If it is due to errors introduced by solving the approximate PDE given in eq 23, then we may have to retreat back to the full PDE without any terms neglected. We may have to retreat even further and formulate an altogether different scheme for choosing our G_k in order to improve the stability and accuracy of our algorithm.

Appendix B. The First-Order Limit

In this appendix, we shall show that our choice for G_k leads to first-order perturbation theory in the limit of small perturbations. To do so, we first need to determine how to string together the infinitesimal, short-time generating functions to form the final generating function.

Consider then the following sets of action-angle variables: $(\mathbf{I}_0,\phi_0)$, $(\mathbf{I}_1,\phi_1)$, $(\mathbf{I}_2,\phi_2)$, at times t, $t + \mathrm{d}t$, $t + 2\mathrm{d}t$, respectively. These action-angle variables are connected by generating functions $S_1(\mathbf{I}_1,\phi_0)$, $S_2(\mathbf{I}_2,\phi_1)$ with

$$S_1(\mathbf{I}_1,\phi_0) = \mathbf{I}_1\cdot\phi_0 + \mathrm{d}tG_1(\mathbf{I}_1,\phi_0) \tag{B1}$$

$$S_2(\mathbf{I}_2,\phi_1) = \mathbf{I}_2\cdot\phi_1 + \mathrm{d}tG_2(\mathbf{I}_2,\phi_1) \tag{B2}$$

Therefore,

$$\mathbf{I}_0 = \mathbf{I}_1 + \mathrm{d}t\nabla_{\phi_0}G_1(\mathbf{I}_1,\phi_0) \tag{B3}$$

$$\phi_1 = \phi_0 + \mathrm{d}t\nabla_{\mathbf{I}_1}G_1(\mathbf{I}_1,\phi_0) \tag{B4}$$

$$\mathbf{I}_1 = \mathbf{I}_2 + \mathrm{d}t\nabla_{\phi_1}G_2(\mathbf{I}_2,\phi_1) \tag{B5}$$

$$\phi_2 = \phi_1 + \mathrm{d}t\nabla_{\mathbf{I}_2}G_2(\mathbf{I}_2,\phi_1) \tag{B6}$$

Therefore, working to first-order in dt, we have

$$\begin{aligned}\mathbf{I}_0 &= \mathbf{I}_2 + \mathrm{d}t\nabla_{\phi_1}G_2(\mathbf{I}_2,\phi_1) + \mathrm{d}t\nabla_{\phi_0}G_1(\mathbf{I}_1,\phi_0)\\ &= \mathbf{I}_2 + \mathrm{d}t\nabla_{\phi_0}G_2(\mathbf{I}_2,\phi_0) + \mathrm{d}t\nabla_{\phi_0}G_1(\mathbf{I}_2,\phi_0)\end{aligned} \tag{B7}$$

and,

$$\begin{aligned}\phi_2 &= \phi_0 + \mathrm{d}t\nabla_{\mathbf{I}_1}G_1(\mathbf{I}_1,\phi_0) + \mathrm{d}t\nabla_{\mathbf{I}_2}G_2(\mathbf{I}_2,\phi_1)\\ &= \phi_0 + \mathrm{d}t\nabla_{\mathbf{I}_2}G_1(\mathbf{I}_2,\phi_0) + \mathrm{d}t\nabla_{\mathbf{I}_2}G_2(\mathbf{I}_2,\phi_0)\end{aligned} \tag{B8}$$

Thus, the generating function from t to $t + 2\mathrm{d}t$ is just $G_3(\mathbf{I}_2,\phi_0) = G_1(\mathbf{I}_2,\phi_0) + G_2(\mathbf{I}_2,\phi_0)$. As long as we are working in the weakly perturbed limit, so that first-order perturbation theory applies, we obtain that our overall generating function $G(\mathbf{I},\theta)$ is given by

$$G(\mathbf{I},\phi) = \int_0^T G_t(\mathbf{I},\theta)\mathrm{d}t \tag{B9}$$

where G_t is the infinitesimal generating function from t to $t + \mathrm{d}t$.

Now that we know how to string together the short-time generating functions, we can determine the form for the final generating function. In the weakly perturbed limit we showed that $\partial H_n/\partial t = -2\pi(\mathbf{n}\cdot\nabla_{\mathbf{I}}H_0)G_n = -8\pi^2(\mathbf{n}\cdot\nabla_{\mathbf{I}}H_0)^2H_n$. Note that $H_0(\mathbf{I})$ remains constant for all $\mathbf{I}$, and so the solution to our differential equation is simply

$$H_n(\mathbf{I},t) = H_n^0(\mathbf{I})\mathrm{e}^{-8\pi^2(\mathbf{n}\cdot\nabla_{\mathbf{I}}H_0)^2t} \tag{B10}$$

Therefore $G_k(\mathbf{I},t) = 4\pi H_k^0(\mathbf{k}\cdot\nabla_{\mathbf{I}}H_0)\mathrm{e}^{-8\pi^2(\mathbf{k}\cdot\nabla_{\mathbf{I}}H_0)^2t}$, $\mathbf{k} \neq 0$. Because $G_k(\mathbf{I},t)$ starts out at 0, then integrating out to ∞ gives us for our final generating function that $G_k(\mathbf{I}) = H_k^0/2\pi(\mathbf{k}\cdot\nabla_{\mathbf{I}}H_0)$, which is exactly the result from first-order perturbation theory, as claimed.

Of course, the above first-order limit derivation is only valid if the system is nonresonant. Otherwise, our final generating function blows up, taking us out of the first-order regime, so

that our method of stringing together our infinitesimal generating functions is no longer valid. However, first-order perturbation theory is also only valid if the system is nonresonant, and so our gradient descent method does indeed reduce to first-order perturbation theory in the weakly perturbed limit.

References and Notes

(1) Carioli, M.; Heller, E. J.; Moller, K. B. *J. Chem. Phys*. **1997**, *106*, 8564.
(2) Chapman, S.; Garrett, B. C.; Miller, W. H. *J. Chem. Phys*. **1976**, *64*, 502.
(3) Warnock, R. L.; Ruth, R. D. *Physica* **1987**, *26D*, 1.
(4) Heller, E. J. *J. Phys. Chem*. **1995**, *99*, 2625.
(5) Pullen, R. A.; Edmonds, A. R. *J. Phys. A Math. Gen*. **1981**, *14*, L477.
(6) Jaffé, C.; Brumer, P. *J. Chem. Phys*. **1985**, *82*, 2330. Jaffé, C.; Brumer, P. *J. Chem. Phys*. **1988**, *88*, 7603.
(7) Stuchebrukhov,A. A.; Marcus, R. A. *J. Chem. Phys*. **1993**, *98*, 6044.
(8) Edward Ott; *Chaos in Dynamical Systems*; Cambridge University Press: New York, 1993.
(9) Herbert Goldstein; *Classical Mechanics*, 2nd ed.; Addison-Wesley, Reading, MA, 1980.
(10) Press, W. H.; Teukolsky, S. A.; Vetterling, W. T.; Flannery, B. P.; *Numerical Recipes in C*, 2nd ed.; Cambridge University Press: New York, 1992.
(11) Maitra, N. T.; Heller, E. J. *Phys. Rev. A*. **1996**, *54*, 4763.
(12) Leitner, D. M.; Wolynes, P. G. *Phys. Rev. Lett*. **1997**, *79*, 55.
(13) Ramachandran, B.; Kay, K. G. *J. Chem. Phys.* **1993**, *99*, 3659.
(14) Sibert, E. L., III *J. Chem. Phys.* **1988**, *88*, 4378.
(15) Sibert, E. L., III; McCoy, A. B. *J. Chem. Phys*. **1996**, *105*, 469.
(16) Wyatt, R. E. *Adv. Chem. Phys*. **1989**, *73*, 231.
(17) Wyatt, R. E.; Iung, C.; Leforestier, C. *J. Chem. Phys*. **1992**, *75*, 3458; **1992**, *75*, 3477.
(18) Lederman, S. M.; Marcus, R. A. *J. Chem. Phys*. **1988**, *88*, 6312.
(19) Lederman, S. M.; Klippenstein, S. J.; Marcus, R. A. *Chem. Phys. Lett*. **1988**, *146*, 7.